In Vivo Molecular Imaging of Atherosclerotic Lesions in ApoE$^{-/-}$ mice using VCAM-1-Specific, ^{99m}Tc-Labeled Peptidic Sequences

Julien Dimastromatteo [1,2], Alexis Broisat [1,2], Pascale Perret[1,2], Mitra Ahmadi [1,2], Didier Boturyn [2,3], Pascal Dumy [2,3], Daniel Fagret [1,2], Laurent M. Riou [1,2], Catherine Ghezzi [1,2]

[1]INSERM, U1039, Radiopharmaceutiques Biocliniques, Grenoble, France ; [2]UJF-Grenoble 1, Grenoble, France ; [3]Département de Chimie Moléculaire, UMR CNRS-UJF 5250, Grenoble, France

Correspondence & reprints: Laurent M. Riou
Faculté de Médecine, Bâtiment Jean Roget
38700 La Tronche
Phone. 33(0)476 637 509 Fax. 33(0)476 637 142
Email. Laurent.Riou@ujf-grenoble.fr

First Author (fellow) : Julien Dimastromatteo
Faculté de Médecine, Bâtiment Jean Roget
38700 La Tronche
Phone. 33(0)476 637 509
Email. Ju.Dimastro@gmail.com

Word count: 4,956

This research was supported by a grant from the Agence Nationale de la Recherche (ANR – PLAQUIMAG 2010-13 program), the Agence Nationale pour la Recherche et la Technologie (ANRT-CIFRE) and ERAS Labo (Saint Nazaire-les-Eymes, France).

ABSTRACT

Vascular Cell Adhesion Molecule-1 (VCAM-1) plays a major role in the chronic inflammatory processes involved in vulnerable atherosclerotic plaque development. We previously showed that the technetium-labeled HMC-I derived peptide B2702p bound specifically to VCAM-1 and allowed the ex vivo imaging of atherosclerotic lesions in WHHL rabbits. However, B2702p target-to-background ratio was suboptimal for the in vivo imaging of VCAM-1 expression in atherosclerotic lesions. In order to improve the target-to-background ratio, twenty derivatives of B2702p (B2702p1 to B2702p20) were synthesized using the ALA-scan methodology. We hypothesized that technetium-radiolabeled B2702p derivatives might allow the molecular imaging of VCAM-1 expression in an experimental model of atherosclerosis.

Methods – A mouse model of focal atherosclerotic plaque development induced by left carotid artery ligation in $ApoE^{-/-}$ mice was used (n = 82). ^{99m}Tc-B2702p and ^{99m}Tc-B2702p1 to ^{99m}Tc-B2702p20 were injected intravenously to anesthetized animals 3 weeks following the ligation. Whole-body planar image acquisition was performed for 3 hrs. Single Photon Emission Computed Tomography (SPECT) imaging of 6 additionnal ligated $ApoE^{-/-}$ mice was also performed with ^{99m}Tc-B2702p1. The animals were then euthanized and the biodistribution of ^{99m}Tc-labeled peptides was evaluated by gamma-well counting of excised organs. The expression of VCAM-1 in the ligated and contralateral carotid arteries was evaluated by immunohistology.

Results - A robust VCAM-1 immunostaining was observed in the left carotid atherosclerotic lesions as a consequence of artery ligation whereas no VCAM-1 expression was detected in the contralateral carotid. Among all evaluated

peptides, ^{99m}Tc-B2702p1 exhibited the most favourable properties. By gamma-well counting, there was a significant 2.0-fold increase in ^{99m}Tc-B2702p1 left-to-right carotid artery activity ratio (2.6±0.6) and a 3.4-fold increase in left carotid-to-blood activity ratio (1.4±0.4) in comparison to ^{99m}Tc-B2702p (1.3±0.2 and 0.4±0.1, respectively, P<0.05 for both comparisons). Similarly, planar images quantification indicated a higher left-to-right carotid activity ratio in ^{99m}Tc-B2702p1 than in ^{99m}Tc-B2702p injected mice (1.2±0.1 *vs.* 1.0±0.0, respectively, P<0.05). Finally, a significantly higher ^{99m}Tc-B2702p1 activity in the left than in the right carotid was observed by SPECT imaging (33.3±5.8 *vs.* 25.1±5.3 cpm/mm²/ID, respectively, P<0.05). **Conclusion –** ^{99m}Tc-B2702p1 is a potentially useful radiotracer for the in vivo molecular imaging of VCAM-1 expression in atherosclerotic plaques.

Keywords: VCAM-1, molecular imaging, vulnerable atherosclerotic plaque

INTRODUCTION

Cardiovascular diseases (CVD) represent the first cause of mortality worldwide (*1*), mostly because there is an unmet need for an efficient screening prevention strategy as illustrated by the fact that sudden cardiac death and acute myocardial infarction are the first symptoms of so far asymptomatic atherosclerosis in >50% of CVD patients (*2*). A non invasive test allowing the detection of coronary vulnerable atherosclerotic lesions in asymptomatic patients prior to the occurence of a cardiovascular event would therefore greatly participate to the overall effort aimed at decreasing the burden of cardiovascular diseases (*1-4*). Nuclear molecular imaging would be perfectly suited for this purpose due to the functional nature of the informations provided by this non invasive imaging methodology (*5*). A number of molecular targets have been evaluated for the development of corresponding specific radiolabeled imaging agents (*6*). Among other relevant molecules, Vascular Cell Adhesion Molecule – 1 (VCAM-1) is a well-recognized marker of atherosclerotic plaque vulnerability (*3, 4, 7-9*) since its overexpression was observed over the complete course of vulnerable plaque development (*10, 11*). In addition, the overexpression of VCAM-1 is strictly restricted to areas of plaque development (*7*), and a number of cell types participating to the evolution of a given atherosclerotic lesion towards a vulnerable plaque overexpress VCAM-1, namely luminal endothelial cells (*12*), macrophages (*13*), smooth muscle cells (*14*) as well as intraplaque neovessels (*10*). We have previously investigated the possibility to image VCAM-1 expression in a Watanabe Heritable Hyperlipidemic rabbit model of

atherosclerosis using ^{99m}Tc- and ^{123}I-labeled versions of the VCAM-1 specific, major histocompatibility complex 1 (MHC-1) derived peptide B2702p (*15, 16*). Despite specific binding to aortic atherosclerotic lesions overexpressing VCAM-1 following in vivo injection and ex vivo autoradiographic imaging, the significant circulating blood activity of ^{99m}Tc- and ^{123}I-B2702p prevented in vivo image acquisition. Discrete modifications in the amino acid sequence of a peptide might allow improvements in the in vivo biodistribution properties of the molecule without affecting its binding specificity (*17-19*). We therefore generated twenty derivatives of the previously evaluated B2702p peptide in order to test the hypothesis that limited modifications to the B2702p sequence might provide improvements in the blood elimination kinetics of the tracer while simultaneously retaining VCAM-1 specific binding properties suitable for the in vivo imaging of VCAM-1 expression in an ApoE-/- mouse model of atherosclerosis.

MATERIALS AND METHODS

Peptide Synthesis and Radiolabeling

The peptidic sequences of B2702p1-20 are presented in Table 1. All derivatives were synthesized by Eurogentec (Eurogentec France SASU, Angers, France). The sequence of Tc-B2702p1 mismatch is a random version of that of Tc-B2702p1. The systematic presence of a histidine residue at the N terminal end of all derivatives allowed ^{99m}Tc radiolabeling with [^{99m}Tc$(OH_2)_{(3)}$ $(CO)_{(3)}$] using a tridentate ligand system. The precursor [^{99m}Tc$(OH_2)_{(3)}$ $(CO)_{(3)}$] was synthesized using a tricarbonyl pharmaceuticals Kit (Isolink®,

Mallinckrodt). The kit was reconstituted with 2 GBq of $^{99m}TcO_4^-$ (Schering SA), and incubated at 100°C for 20 minutes prior to pH adjustment to 8.0 using HCl 2N.

1100-1500 MBq of the reconstituted kit were added to 32 nmoles (50 µg) of B2702P1-20 and incubated for 20 min at 80°C. The radiochemical purity was determined using high performance liquid chromatography (HPLC) using a Licrosorb RP-C18 column (Supelco) (5 µm, 4.6x250 mm). The solvent system consisted of H2O–trifluoroacetic acid (TFA) 0.1% (solvent A) and acetonitrile 90%–TFA 0.1% (solvent B) with a flow rate of 1 mL/min. Tracer elution was achieved by applying a gradient of 5% B during 5 min, a linear gradient from 5% to 60% during 15 min and 60% B during 5min before the system returned to the initial conditions within 5 min.

In Vitro Experiments: Fluorescence Polarization

Binding of B2702p1 to VCAM-1 was evaluated in vitro by fluorescence polarization using a fluorescent analog of B2702p1 ([F]-B2702-p1). The fluorescence polarization of a 12.5 nmol/L (100 µL) solution of [F]-B2702p1 was measured in the absence of VCAM-1 or following incremental additions (0.5 µL) of a 13.5 µmol/L solution of the adhesion molecule using a Perkin-Elmer LS 50 spectrometer. Control experiments were conducted by replacing VCAM-1 by bovine serum albumin as a non-specific ligand (BSA, final concentration ranging from 0 – 27 µmol/L). The experiments were performed in triplicate. Anisotropy data (*A*, arbitrary units) was fitted using the formula $A = A_0 + (A_{max}-A_0)*([Target]/(K_d + [Target]))$ for a one-to-one interaction where A_0 represents the anisotropy value in the absence of VCAM-1 and A_{max}

the maximum anisotropy value that was observed in the presence of increasing concentrations of the molecular target (VCAM-1 or BSA) (20). The K_d value for the interaction between [F]-B2702p1 and VCAM-1 or BSA was determined according to the above equation.

Experimental Protocol

Experimental Model.

All experiments were approved by the Animal Care and Use Committee of the Military Research and Health Center (CRSSA, authorization # 2006/37.0), Grenoble, France. All experiments were performed under the supervision of an authorized individual (LMR, authorization #38 05 39). Eighty-two (82) hypercholesterolemic female apoE-/- mice weighing 19.3 ± 0.2 g were obtained from Charles River Laboratories (L'Arbresle, France). The animals were anesthetized using an intraperitoneal injection of xylazine (1/3; 10 mg/kg) and ketamine (2/3; 100 mg/kg). A skin incision was performed at the level of the thyroid gland and the left common carotid artery was ligated near the bifurcation using 5-0 silk (Ethicon). The incision was then sutured and the animals were allowed to return to individual cages.

In Vivo Imaging and Biodistribution Studies.

Three weeks following left carotid artery ligation, the animals were reanesthetized as described above and 34.7 ± 0.8 MBq of tracer were injected through a tail vein. The animals were then placed on the parallel-hole collimator of a small animal dedicated gamma-camera (Gamma-Imager,

Biospace Lab, Paris, France) and planar imaging was performed for 180 min in the list mode using a 125-150 keV energy window with anesthesia being maintained using isoflurane 1%. High-resolution, pinhole SPECT imaging of ^{99m}Tc-B2702p1 and ^{99m}Tc-B2702p was also performed 150 and 210 min following tracer injection using the same imaging system (n = 6 and 4, respectively).

Regions of interest (ROIs) were drawn on the left carotid lesional area as well as on the contralateral vessel on both planar and tomographic images and tracer activity was expressed as counts per minutes (cpm) per square millimeter (mm^2) per injected MBq (cpm/mm^2/MBq). Image reconstruction was performed using γ–acquisition software and and an Ordered-Subsets-Expectation- Maximization reconstruction algorithm. At the end of image acquisition, the animals were euthanized by an overdose of intraperitoneally administered pentobarbital and samples from the left and right carotid arteries, aorta, lung, liver, spleen, blood, adipose tissue and skeletal muscle were obtained together with the heart, kidney, and thyroid. The blood kinetics of ^{99m}Tc-B2702p1 were also determined following i.v. injection as described above and euthanasia followed by blood withdrawal and left & right carotid excision at 15 (n=3) and 60 min (n=3) post-injection. The tissue samples and organs were quickly rinsed and weighted and their activities were assessed using a gamma-well counter (Cobra II, Packard Instruments) and a 100-168 keV energy window. Tracer activity was expressed as % of the injected dose per gram of wet weight (%ID/g). Urinary and blood sampling was also performed in order to assess the stability of the injected tracers using HPLC as decribed above.

Histology & Immunohistology.

Standard trichrome HES staining (Haematoxylin, Erythrosine, Safran) for nuclei, cytoplasm and fibrosis staining, and immunohistological staining of VCAM-1 and Mac-2 were performed using previously described procedures (*21*).

Statistical Analysis.

Values are presented as mean ± SD. Statistical computations were performed using SYSTAT software (SPSS, Inc.). Between-groups comparisons were performed using unpaired t-test and Kruskal-Wallis test whereas within-group analysis was performed using one-way analysis of variance and Wilcoxon sign-rank test. P values$\leq$0.05 were considered statistically significant.

RESULTS

Histology & Immunohistology

As shown in Figure 1, left carotid artery ligation resulted in atherosclerotic lesion development at the site of occlusion. Positive VCAM-1 and Mac-2 immunostainings were observed in atherosclerotic lesions developing at the site of left carotid artery ligation but not in contralateral, right carotid arteries nor in vessels from sham-operated animals. In addition, immunohistochemical stainings indicated no signs of post-surgery skin inflammation at the time of

tracer injection as a consequence of the three-week time interval between surgery and image acquisition allowing complete healing of the incision site.

Biodistribution Studies

As indicated in Table 1, the radiolabeling of all peptidic sequences was successfully performed with a RCP>88% with the exception of B2702p5 (RCP ~ 50%) which was therefore not further considered for evaluation. All radiotracers displayed good urinary stability with the exception of B2702p7 and B2702p16. The 180-min biodistribution of all radiotracers is presented in Table 2. The kidneys represented the preferential route of excretion for all tracers except for Tc-B2702p1 mismatch, Tc-B2702p7, and Tc-B2702p9 for which the hepatobiliary route was equally involved. Significant thyroid uptake likely indicative of radiolabeling instability following in vivo injection was observed for Tc-B2702p, Tc-B2702p11, Tc-B2702p12, Tc-B2702p13, Tc-B2702p14, Tc-B2702p15, and Tc-B2702p18. Tc-B2702p1 and Tc-B2702p18 left carotid activities were significantly higher than that observed in the right carotid artery. Shown in Figure 2 are the left-to-right carotid activity ratios (A) and left carotid-to-blood activity ratios (B) for all radiotracers. Tc-B2702p1 left-to-right carotid and left carotid-to-blood activity ratios at 180 min (2.6 ± 0.6 and 1.4 ± 0.4, respectively) were significantly higher than those of Tc-B2702p (1.3 ± 0.2 and 0.4 ± 0.1, respectively) and Tc-B2702p1 mismatch (1.1 ± 0.0 and 0.5 ± 0.1, respectively). In addition, Tc-B2702p1 was the only tracer with a left carotid-to-blood activity ratio >1. Finally, the blood kinetics of Tc-B2702p1 were best fitted using a biexponential fit with half-lives of 13 min and 187 min (Figure 3). Also shown on Figure 3 is the comparison between

blood, left and right carotid activities indicating that 180 min post-injection represented the optimal time point for in vivo imaging.

In Vivo Imaging

Representative in vivo planar images acquired between 150 and 180 min following the injection of Tc-B2702p1, Tc-B2702p1 mismatch and Tc-B2702p are displayed in Figure 4A. The results indicated that the atherosclerotic lesion expressing VCAM-1 and developing on the left carotid artery following vessel ligation was readily visualized following the injection of Tc-B2702p1, but not that of Tc-B2702p1 mismatch and Tc-B2702p. Results from in vivo planar image quantification are shown in Figure 4B. Tc-B2702p1 left-to-right carotid activity ratio (1.2 ± 0.1) was significantly higher than those of Tc-B2702p (1.0 ± 0.0) and Tc-B2702p1 mismatch (1.0 ± 0.0). These results were further confirmed following in vivo pinhole SPECT imaging of Tc-B2702p1 left carotid lesion uptake. As shown in Figure 5, Tc-B2702p1 left carotid activity was higher than that observed in the contralateral vessel in all animals (mean values, 2.2 ± 0.4 cpm/mm²/MBq and 1.4 ± 0.3 cpm/mm²/MBq, respectively, $P<0.01$), resulting in a left-to-right carotid activity ratio of 1.6 ± 0.1 following injection of Tc-B2702p1.

In Vitro Experiments

Results from fluorescence polarisation experiments are presented in Figure 6. An increasing anisotropy value was observed in the presence of increasing VCAM-1 concentrations and a plateau was reached. A Kd value of 15×10^{-6} mol/L for the interaction between VCAM-1 and [F]-B2702p1 was determined

assuming a one-to-one interaction (see Materials and methods). This value was ~40-fold lower than that observed in the presence of BSA ($5.95x10^{-4}$ mol/l).

DISCUSSION

^{99m}Tc-B2702p has been previously validated as a tracer of VCAM-1 expression in a WHHL rabbit model of atherosclerosis (*15*). However, the suboptimal blood kinetics of the tracer prevented in vivo image acquisition. In the present study, we hypothesized that the in vivo kinetics of ^{99m}Tc-B2702p might be improved by discrete modifications of the amino acid sequence of the peptide, thereby allowing the in vivo imaging of VCAM-1 expression. Derivated peptides were therefore initially generated following an ALA-scan methodology consisting in the systematic replacement of the original residues with an Ala in each position of the peptide. Additional modifications were also performed by inverting two residues prior to reiterating the ALA-scan methodology on the pre-modified peptide (Table 1). The ALA-scan strategy has been previously used to investigate the structure-activity relationship of peptidic receptor antagonists (*17*). ALA-scan modifications have been described to either decrease, have no effect, or possibly increase the potency and metabolic stability of the peptide being modified (*17-19*).

Twenty peptides were therefore generated from the original B2702p sequence and labeled with ^{99m}Tc using the Isolink® method for biological evaluation on an ApoE-/- mouse model of atherosclerosis. Briefly, a focal atherosclerotic lesion was induced in hypercholesterolemic ApoE-/- animals by left carotid artery ligation. This model was previously validated as suitable for the experimental evaluation of potential radiotracers of atherosclerotic plaques

(*22*). In the present study, we verified that VCAM-1 expression occurred at the site of plaque development but not in the contralateral vessel as illustrated by immunohistology experiments. The overexpression of VCAM-1 was concomitent to the presence of macrophages, thereby indicative of the occurrence of an inflammatory process similar to that observed in vulnerable lesions.

The results from biodistribution studies indicated that the highest left-to-right carotid and left carotid-to-blood activity ratios were obtained following the injection of Tc-B2702p1. In addition, Tc-B2702p1 was the only derivative with a left carotid-to-blood activity ratio >1, suggesting that the tracer target-to-background ratio would be suitable for the in vivo imaging of VCAM-1 expression. In vivo planar imaging studies confirmed this hypothesis. Indeed, the atherosclerotic lesion developing at the site of left carotid artery ligation was readily identified following injection of Tc-B2702p1. Tc-B2702p injection resulted in significant thyroid activity as indicated by the biodistribution data presented in Table 2, which might indicate suboptimal *in vivo* tracer stability whereas thyroid activity remained very low following Tc-B2702p1 injection, in accordance with good *in vivo* tracer stability. However, high Tc-B2702p circulating tracer activity and small thyroid dimensions likely precluded thyroid visualization on planar images whereas low Tc-B2702p1 circulating and thyroid activities allowed the imaging of Tc-B2702p1 specific uptake in atherosclerotic lesions. High-resolution tomographic imaging experiments yielded results similar to those observed using planar imaging, with a systematically higher tracer activity in the atherosclerotic lesion located on the left carotid artery than in the contralateral vessel leading to a mean left-

to-right carotid tracer activity ratio of 1.6 ± 0.1. The specificity of Tc-B2702p1 binding to VCAM-1 in vivo was demonstrated by the fact that atherosclerotic plaque imaging could not be performed following the injection of Tc-B2702p1 mismatch, which peptidic sequence consisted in similar amino acids in a random peptidic sequence.

The affinity of the B2702p1 peptidic sequence for VCAM-1 was determined with fluorescence polarization using a similar methodology to that previously used to evaluate the Kd value corresponding to the interaction between B2702p and VCAM-1 (15). The observed Kd value for the interaction between B2702p1 and VCAM-1 was ~15 µmol/L, a value ~50-fold higher than that observed for B2702, consistent with the observation that a decrease in ligand affinity is frequently observed when using the ALA-scan methodology (*17*). Several peptidic VCAM-1 ligands were recently described. In vitro phage display allowed the selection of the multimodal nanoparticle VNP (*23*), whereas in vivo phage display led to the discovery of VINP-28, a linear sequence which allowed the in vivo imaging of atherosclerotic lesions using MRI and optical imaging (*24*). More recently, a tetrameric peptide of nanomolar affinity for VCAM-1 and consisting of 4 VINP-28 sequences allowed the nuclear imaging of apoE-/- mouse atherosclerotic lesion following radiolabelling with ^{18}F (*25*). In addition, the recently described R832 short peptidic sequence was obtained using the in vitro phage display methodology as well. The peptide displayed a micromolar affinity for VCAM-1 and allowed the in vivo detection of VCAM-1 expression following conjugation to Gd-DOTA and MR imaging (*26*). Taken altogether, the results from the above

mentioned studies suggest that a wide range of affinities might be suitable for the non invasive imaging of molecular targets.

The affinity of the peptidic sequence B2702p1 described in the present study for VCAM-1 is similar to that of R832. Importantly, the discrete amino acid modifications that led to the B2702p1 peptide from the original B2702p sequence led to a decreased circulating activity for Tc-B2702p1 when compared to Tc-B2702p. Indeed, Tc-B2702p1 blood activity was >6-fold lower than that observed for Tc-B2702p, leading to a target-to-background ratio suitable for in vivo imaging. On the other hand, the elevated circulating blood activity of Tc-B2702p together with a suboptimal stability of the tracer following in vivo injection as illustrated by the significant thyroid activity prevented the successful obtention of in vivo images of VCAM-1 expression.

CONCLUSION

B2702p1 was selected among 20 ALA-scan derivatives of the previously described peptidic sequence B2702p as the tracer allowing the in vivo imaging of VCAM-1 expression in a murine model of atherosclerosis following radiolabeling with 99mTc. Further clinical studies are needed to determine the potential of the tracer for the detection of vulnerable atherosclerosis in patients.

ACKNOWLEDGEMENTS

The authors acknowledge Anatomopathology Service and Nuclear Service staff (CHU, Grenoble, France) for the assistance with histology and radiolabeling and René Bontron for his assistance with animals. This research was supported by a grant from the Agence Nationale de la Recherche (ANR – PLAQUIMAG 2010-13 program), the Agence Nationale pour le Recherche et la Technologie (ANRT-CIFRE) and ERAS Labo.

REFERENCES

1. Roger VL, Go AS, Lloyd-Jones DM, et al. Heart disease and stroke statistics - 2011 update: a report from the American Heart Association. *Circulation*. 2011;123:e18-e209.

2. Naghavi M, Falk E, Hecht HS, et al. From vulnerable plaque to vulnerable patient--Part III: Executive summary of the Screening for Heart Attack Prevention and Education (SHAPE) Task Force report. *Am J Cardiol*. 2006;98:2H-15H.

3. Naghavi M, Libby P, Falk E, et al. From vulnerable plaque to vulnerable patient: a call for new definitions and risk assessment strategies: Part II. *Circulation*. 2003;108:1772-1778.

4. Naghavi M, Libby P, Falk E, et al. From vulnerable plaque to vulnerable patient: a call for new definitions and risk assessment strategies: Part I. *Circulation*. 2003;108:1664-1672.

5. Sadeghi MM, Glover DK, Lanza GM, Fayad ZA, Johnson LL. Imaging atherosclerosis and vulnerable plaque. *J Nucl Med*. 2010;51 (Suppl 1):51S-65S.

6. Riou LM, Broisat A, Dimastromatteo J, Pons G, Fagret D, Ghezzi C. Pre-clinical and clinical evaluation of nuclear tracers for the molecular imaging of vulnerable atherosclerosis: an overview. *Curr Med Chem*. 2009;16:1499-1511.

7. Iiyama K, Hajra L, Iiyama M, et al. Pattern of vascular cell adhesion molecule-1 and intercellular adhesion molecule-1 expression in rabbit and mouse atherosclerotic lesions and at sites predisposed to lesion formation. *Circ Res*. 1999;85:199–207.

8. Ley K, Huo Y. VCAM-1 is critical in atherosclerosis. *J Clin Invest.* 2001;107:1209–1210.

9. Cybulsky MI, Liyama K, Li H, Zhu S, et al. A major role for VCAM-1 but not ICAM-1, in early atherosclerosis. *J Clin Invest*. 2001;107:1255–1262.

10. O'Brien KD, Allen MD, McDonald TO, et al. Vascular cell adhesion molecule-1 is expressed in human coronary atherosclerotic plaques. *J Clin Invest*. 1993;92:945–951.

11. O'Brien KD, McDonald TO, Chait A, Allen MD, Alpers CE. Neovascular expression of E-selectin, intercellular adhesion molecule-1 and vascular adhesion molecule-1 in human atherosclerosis and their relation to intimal leucocyte content. *Circulation.* 1996;93:672–682.

12. Ramos CL, Huo Y, Jung U, et al. Direct demonstration of P-selectin- and VCAM-1-dependent mononuclear cell rolling in early atherosclerotic lesions of apolipoprotein E-deficient mice. *Circ Res*. 1999;84:1237-1244.

13. Davies MJ, Gordon JL, Gearing AJ, Pigott R, Woolf N, Katz D, Kyriakopoulos A. The expression of the adhesion molecules ICAM-1, VCAM-1, PECAM, and E-selectin in human atherosclerosis. *J Pathol*. 1993;171:223-229.

14. Orr AW, Hastings NE, Blackman BR, Wamhoff BR. Complex regulation and function of the inflammatory smooth muscle cell phenotype in atherosclerosis. *J Vasc Res*. 2010;47:168-180.

15. Broisat A, Riou LM, Ardisson V, et al. Molecular imaging of vascular cell adhesion molecule-1 expression in experimental atherosclerotic plaques with radiolabelled B2702-p. *Eur J Nucl Med Mol Imaging*. 2007;34:830-840.

16. Ling X, Tamaki T, Xiao Y, et al. An immunosuppressive and anti-inflammatory HLA class Iderived peptides binds vascular cell adhesion molecule-1. *Transplantation*. 2000;70:662–667.

17. Quartara L, Ricci R, Meini S, et al. Ala scan analogues of HOE 140. Synthesis and biological activities. *Eur J Med Chem*. 2000;35:1001-1010.

18. Marrakchi N, Mabrouk K, Regaya I, et al. Lebetin peptides: potent platelet aggregation inhibitors. *Haemostasis*. 2001;31:207-210.

19. Van Craenenbroeck M, Gregoire F, De Neef P, Robberecht P, Perret J. Ala-scan of ghrelin (1-14): interaction with the recombinant human ghrelin receptor. *Peptides*. 2004;25:959-965.

20. Sörme P, Kahl-Knutsson B, Huflejt M, Nilsson UJ, Leffler H. Fluorescence polarization as an analytical tool to evaluate galectin-ligand interactions. *Anal Biochem* 2004;334:36–47.

21. Broisat A, Toczek J, Mesnier N, et al. Assessing low levels of mechanical stress in aortic atherosclerotic lesions from apolipoprotein E-/- mice. *Arterioscler Thromb Vasc Biol*. 2011;31:1007-1010.

22. Schäfers M, Riemann B, Kopka K, et al. Scintigraphic imaging of matrix metalloproteinase activity in the arterial wall in vivo. *Circulation*. 2004;109:2554-2559.

23. Kelly KA, Allport JR, Tsourkas A, Shinde-Patil VR, Josephson L, Weissleder R. Detection of vascular adhesion molecule-1 expression using a novel multimodal nanoparticle. *Circ Res*. 2005;96:327-336.

24. Nahrendorf M, Jaffer FA, Kelly KA, et al. Noninvasive vascular cell adhesion molecule-1 imaging identifies inflammatory activation of cells in atherosclerosis. *Circulation*. 2006;114:1504-1511.

25. Nahrendorf M, Keliher E, Panizzi P, et al. 18F-4V for PET-CT imaging of VCAM-1 expression in inflammatory atherosclerosis. *JACC Cardiovasc Imaging*. 2009;2:1213–1222.

26. Burtea C, Laurent S, Port M, et al. Magnetic resonance molecular imaging of vascular cell adhesion molecule-1 expression in inflammatory lesions using a peptide-vectorized paramagnetic imaging probe. *J Med Chem*. 2009;52:4725-4742.

FIGURE LEGENDS

FIGURE 1. Histological (HES) and immunohistological stainings of VCAM-1 and Mac-2 expressions in ApoE-/- mouse carotid vessels. Histo- and immunohistochemistry was performed on adjacent transverse sections of atherosclerotic lesions from ligated left carotid arteries (A – E), with magnifications centered on the intimal and adventitial areas (F – J and K – O, respectively) as well as on unligated left carotid arteries from sham-operated ApoE-/- animals (P - T) and on contralateral, right carotid arteries (U - Y). Positive VCAM-1 and Mac-2 immunostainings were observed in atherosclerotic lesions developing at the site of left carotid artery ligation but not in vessels from sham-operated animals and right carotid arteries. The specificity of immunostainings was assessed by performing control experiments in the absence of VCAM-1- and Mac-2-specific primary antibodies (w/o VCAM-1 Ab and w/o MAC-2 Ab). *, vessel lumen.

FIGURE 2. Left-to-right carotid (A) and left carotid-to-blood (B) activity ratios of Tc-labeled peptidic sequences as determined by gamma-well counting at 180 min following intravenous tracer injection. *P<0.05 vs. Tc-B2702p, †P<0.05 vs. Tc-B2702p1 mismatch.

FIGURE 3. Time-activity curves of Tc-B2702p1 in the blood and left & right carotid arteries at 15, 60, and 180 min following intravenous injection of the tracer.

FIGURE 4. A, Representative planar images of apoE-/- mouse with left carotid artery ligation at 180 min following the injection of Tc-B2702p1 (left), Tc-B2702p1 mismatch (middle), and Tc-B2702p (right). The corresponding left-to-right carotid tracer activity ratios are indicated in parenthesis; B, Tc-B2702p1, Tc-B2702p1 mismatch, and Tc-B2702p left-to-right carotid activity ratios from in vivo planar image quantification. *P<0.05 vs. Tc-B2702p; †P<0.05 vs. Tc-B2702p1 mismatch.

FIGURE 5. A, Representative pinhole SPECT image of Tc-B2702p1 (left) and ^{99m}Tc-B2702p (right) activity at the level of the atherosclerotic lesion developing at the site of left carotid artery ligation in an apoE-/- mouse. The corresponding left-to-right carotid tracer activity ratios are indicated in parenthesis; B, Left & right Tc-B2702p1 (left) and ^{99m}Tc-B2702p (right) carotid activities from in vivo pinhole SPECT image quantification. *, P<0.05 vs. right carotid tracer activity.

FIGURE 6. Anisotropy values from [F]-B2702p1 in the presence of increasing concentrations of recombinant human VCAM-1. Results from control experiments performed in the absence of VCAM-1 and in the presence of the non-specific target BSA are shown in the insert.

Table 1. **Peptidic sequence, radiochemical purity, and urinary stability of Tc-B2702p1-20 peptides.**

Tracer	Peptidic sequence	RCP (%)	Stability (%)
^{99m}Tc-B2702p	H_2N-HGR ENL RIA LRY- COOH	90	93
^{99m}Tc-B2702p1	H_2N-HGR ANL RIL ARY- COOH	92	94
^{99m}Tc-B2702p1mis.	H2N- HGL RAY IRA RNL -COOH	90	89
^{99m}Tc-B2702p2	H_2N-HGR ENL AIL ARY- COOH	95	96
^{99m}Tc-B2702p3	H_2N-HGR ENL RIL ARA- COOH	97	83
^{99m}Tc-B2702p4	H_2N-HGR ENL RIL AAY- COOH	95	92
^{99m}Tc-B2702p5	H_2N-HGR ENL RIL ARY- COOH	50	N/D
^{99m}Tc-B2702p6	H_2N-HGR ENA RIL ARY- COOH	93	95
^{99m}Tc-B2702p7	H_2N-HGA ENL RIL ARY- COOH	95	50
^{99m}Tc-B2702p8	H_2N-HGR ENL RIA ARY- COOH	80	84
^{99m}Tc-B2702p9	H_2N-HGR EAL RIL ARY- COOH	95	97
^{99m}Tc-B2702p10	H_2N-HGR ENL RIL ARY- COOH	95	99
^{99m}Tc-B2702p11	H_2N-HGA ENL RIA LRY- COOH	97	82
^{99m}Tc-B2702p12	H_2N-HGR ANL RIA LRY- COOH	88	80
^{99m}Tc-B2702p13	H_2N-HGR EAL RIA LRY- COOH	96	79
^{99m}Tc-B2702p14	H_2N-HGR ENA RIA LRY- COOH	96	76
^{99m}Tc-B2702p15	H_2N-HGR ENL AIA LRY- COOH	96	85
^{99m}Tc-B2702p16	H_2N-HGR ENL RAA LRY- COOH	91	70
^{99m}Tc-B2702p17	H_2N-HGR ENL RIA LAY- COOH	90	80
^{99m}Tc-B2702p18	H_2N-HGR ENL RIA LRA- COOH	88	81
^{99m}Tc-B2702p19	H_2N-HGR ANL RIL ARA- COOH	88	79
^{99m}Tc-B2702p20	H_2N-HGR ANL RIL AAY- COOH	92	78

Table 2. Biodistribution of Tc-B2702p1-20 at 180 min following injection to ApoE-/- mice with left carotid artery ligation.

Tracer	Heart	Aorta	Lung	Liver	Spleen	Kidney	Fat	Muscle	Blood	Thyroid	L. carotid	R. carotid
Tc-B2702p	1.5±0.1	2.7±0.4	3.9±0.4	10.6±2.6	2.2±0.3	69.0±13.0	1.0±0.2	1.2±0.2	5.7±0.6	9.7±3.0	2.4±0.4	1.8±0.3
Tc-B2702p1	0.3±0.1	0.5±0.1	0.8±0.1	3.1±0.6	1.6±0.7	4.6±0.5	0.2±0.0	0.1±0.0	0.9±0.2†	0.7±0.2	1.3±0.4*	0.5±0.1†
Tc-B2702p1mis	0.7±0.2	1.7±0.7	1.7±0.4	22.1±5.9	0.8±0.1	15.5±4.2	0.5±0.2	0.5±0.1	2.4±0.8	1.1±0.4	1.2±0.6	1.2±0.6
Tc-B2702p2	0.3±0.1	0.9±0.6	0.8±0.3	2.7±0.3	1.4±0.4	13.4±1.9	0.3±0.2	0.2±0.1	0.9±0.3†	1.3±0.1	0.5±0.2†	0.3±0.1†
Tc-B2702p3	0.4±0.1	0.7±0.2	0.9±0.2	4.2±0.6	0.8±0.2	33.1±0.7	0.3±0.1	0.2±0.1	1.3±0.3†	0.6±0.1	0.5±0.1†	0.4±0.1†
Tc-B2702p4	0.3±0.1	0.6±0.3	0.6±0.2	4.7±0.9	0.6±0.2	26.2±5.1	0.2±0.1	0.2±0.1	0.9±0.4†	0.6±0.2	0.7±0.4†	0.2±0.1†
Tc-B2702p6	0.3±0.0	0.6±0.0	0.7±0.0	5.9±1.0	0.5±0.0	8.2±0.7	0.2±0.0	0.1±0.0	1.1±0.1†	1.5±0.3	0.5±0.1†	0.4±0.2†
Tc-B2702p7	0.4±0.0	0.7±0.1	0.9±0.1	8.2±0.4	1.0±0.3	8.0±1.3	0.2±0.0	0.2±0.0	1.3±0.1†	1.9±0.7	0.4±0.2†	0.4±0.2†
Tc-B2702p8	0.3±0.1	0.7±0.1	0.9±0.1	6.9±1.6	0.8±0.2	20.6±10.8	0.2±0.1	0.2±0.1	1.2±0.3†	1.6±0.6	0.4±0.1†	0.2±0.1†
Tc-B2702p9	0.1±0.0	0.3±0.0	0.4±0.0	2.1±0.1	0.4±0.1	2.2±0.2	0.1±0.0	0.1±0.0	0.4±0.0†	0.4±0.0	0.1±0.0†	0.1±0.0†
Tc-B2702P10	0.5±0.3	0.3±0.0	0.4±0.1	2.8±0.5	0.4±0.1	23.6±3.7	0.1±0.0	0.1±0.0	0.4±0.0†	0.3±0.0	0.1±0.0†	0.4±0.2†
Tc-B2702p11	1.8±0.1	2.7±0.1	3.6±0.3	10.8±0.6	2.9±0.1	19.2±0.8	1.5±0.3	0.6±0.1	6.7±0.4	14.2±6.9	2.1±0.3	1.9±0.7
Tc-B2702p12	0.4±0.1	2.8±0.9	4.2±1.5	5.5±0.6	3.1±0.2	36.9±11.4	0.8±0.1	0.8±0.4	4.4±1.2	8.8±2.8	2.1±0.9	1.4±0.4
Tc-B2702p13	1.6±0.3	2.3±0.3	3.3±0.4	8.0±0.6	2.9±0.4	22.7±7.5	0.8±0.3	0.5±0.1	5.9±0.5	11.0±3.2	1.7±0.3	1.8±0.4
Tc-B2702p14	2.5±0.7	3.2±0.6	5.7±1.4	12.7±2.4	3.7±1.0	34.6±1.9	0.8±0.1	0.7±0.2	10.7±2.2	15.9±2.6	2.2±0.2	2.2±0.2
Tc-B2702p15	4.5±0.3	5.2±0.1	11.2±0.7	18.1±0.7	6.4±0.2	34.0±4.4	1.6±0.7	1.2±0.1	16.4±0.9	6.3±1.1	3.3±0.7	1.9±0.5
Tc-B2702p16	0.3±0.0	0.6±0.1	0.9±0.1	3.4±0.4	1.2±0.1	98.9±18.1	0.4±0.1	0.2±0.0	1.0±0.1†	1.7±0.2	0.4±0.0†	0.4±0.2†
Tc-B2702p17	0.4±0.1	0.6±0.2	1.2±0.5	3.5±1.2	1.6±0.7	85.3±25.7	0.3±0.1	0.3±0.2	1.3±0.4†	2.8±0.4	0.4±0.1†	0.2±0.1†
Tc-B2702p18	0.5±0.1	2.5±0.4	3.2±0.5	6.3±1.5	2.3±0.7	63.9±17.2	1.2±0.5	0.7±0.0	5.9±1.0	18.8±2.7	2.0±0.2*	1.0±0.1†
Tc-B2702p19	0.5±0.1	0.9±0.3	1.3±0.2	5.5±0.5	1.5±0.1	15.2±6.0	0.2±0.0	0.3±0.0	2.0±0.5†	1.9±1.5	0.7±0.1†	1.1±0.5
Tc-B2702p20	0.6±0.2	1.4±0.4	1.2±0.3	6.1±1.1	1.0±0.4	11.1±2.0	0.2±0.1	0.2±0.1	2.2±0.6†	0.5±0.2	0.9±0.1†	1.2±0.8

The values (presented as mean ± standart error of the mean) are expressed as %ID/g. L., left; R., right; *, P<0.05 vs. Right Carotid; †, P<0.05 vs. Tc-B2702p.

FIGURE 1

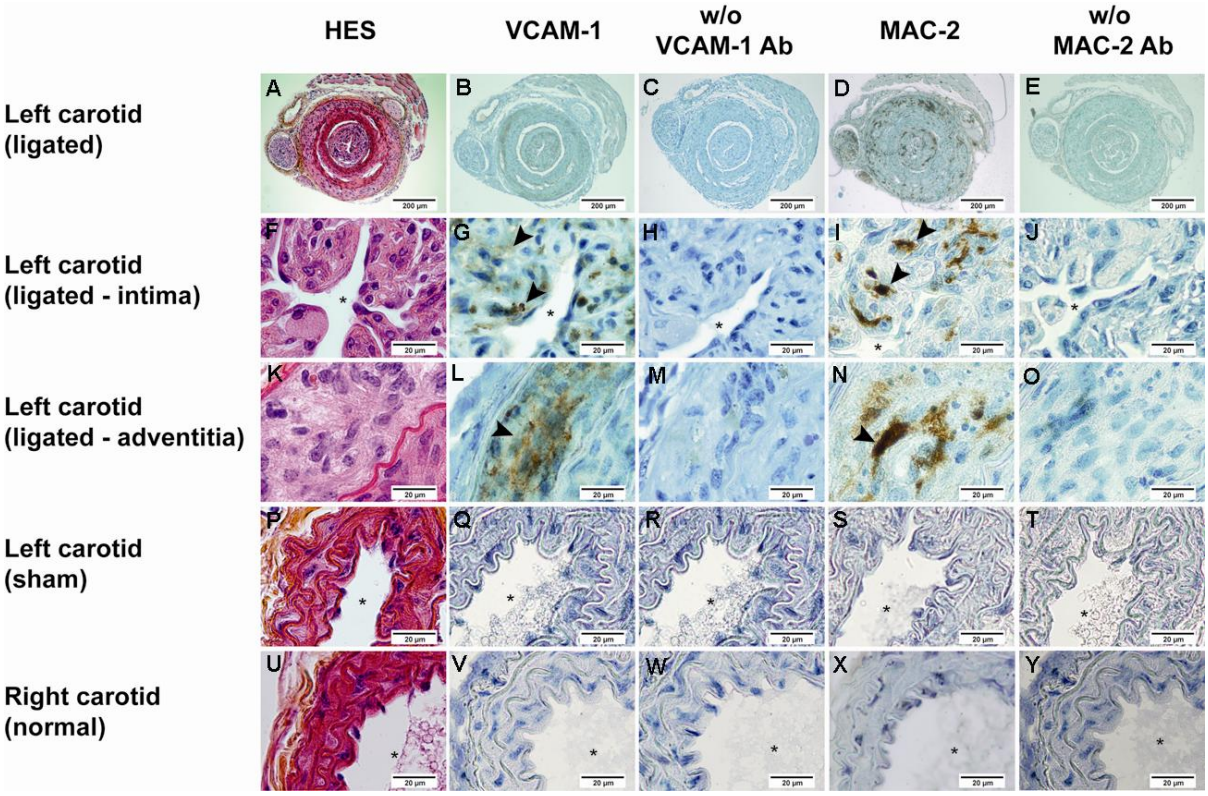
HES
VCAM-1
w/o VCAM-1 Ab
MAC-2
w/o MAC-2 Ab
Left carotid (ligated)
Left carotid (ligated - intima)
Left carotid (ligated - adventitia)
Left carotid (sham)
Right carotid (normal)
A
B
C
D
E
F
G
H
I
J
K
L
M
N
O
P
Q
R
S
T
U
V
W
X
Y

FIGURE 2

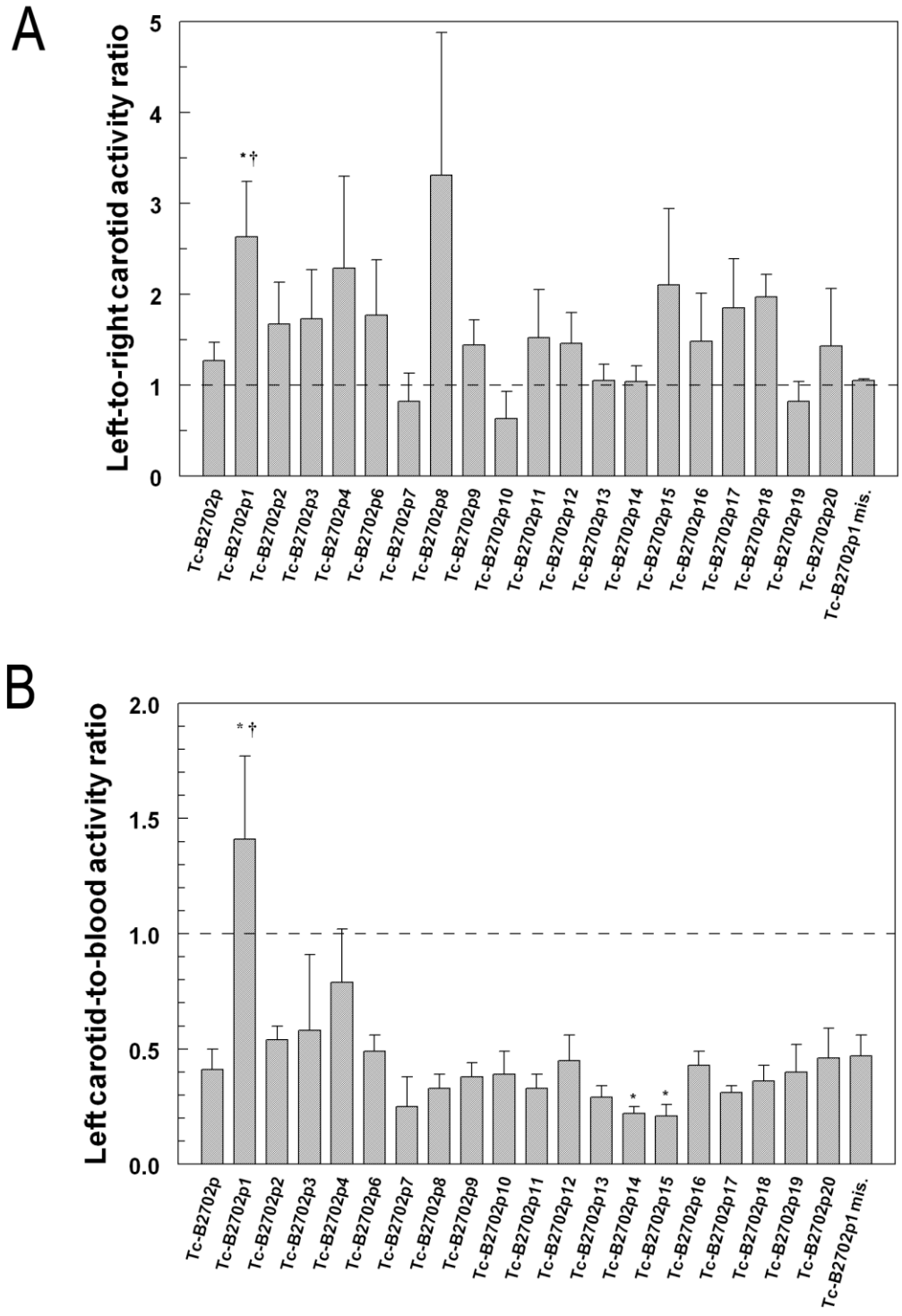
A
Left-to-right carotid activity ratio
0
1
2
3
4
5
* †
Tc-B2702p
Tc-B2702p1
Tc-B2702p2
Tc-B2702p3
Tc-B2702p4
Tc-B2702p6
Tc-B2702p7
Tc-B2702p8
Tc-B2702p9
Tc-B2702p10
Tc-B2702p11
Tc-B2702p12
Tc-B2702p13
Tc-B2702p14
Tc-B2702p15
Tc-B2702p16
Tc-B2702p17
Tc-B2702p18
Tc-B2702p19
Tc-B2702p20
Tc-B2702p1 mis.
B
Left carotid-to-blood activity ratio
0.0
0.5
1.0
1.5
2.0
* †
*
*
Tc-B2702p
Tc-B2702p1
Tc-B2702p2
Tc-B2702p3
Tc-B2702p4
Tc-B2702p6
Tc-B2702p7
Tc-B2702p8
Tc-B2702p9
Tc-B2702p10
Tc-B2702p11
Tc-B2702p12
Tc-B2702p13
Tc-B2702p14
Tc-B2702p15
Tc-B2702p16
Tc-B2702p17
Tc-B2702p18
Tc-B2702p19
Tc-B2702p20
Tc-B2702p1 mis.

FIGURE 3

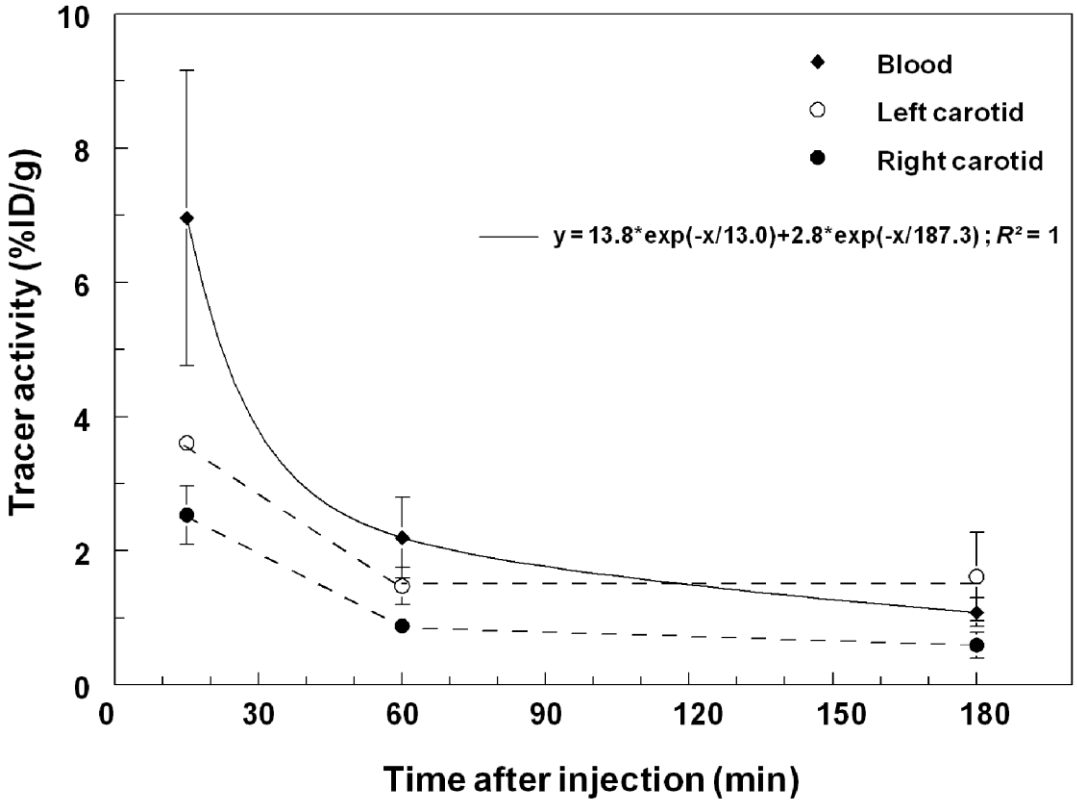
Blood
Left carotid
Right carotid
y = 13.8*exp(-x/13.0)+2.8*exp(-x/187.3) ; R² = 1
Tracer activity (%ID/g)
Time after injection (min)
0
2
4
6
8
10
0
30
60
90
120
150
180

FIGURE 4

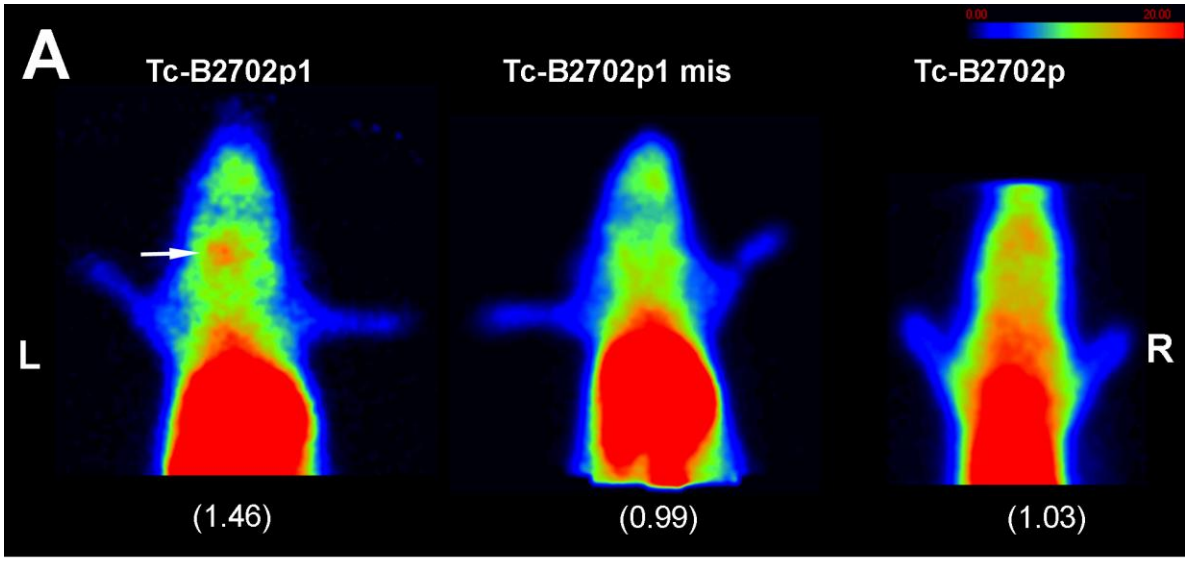
A
Tc-B2702p1
Tc-B2702p1 mis
Tc-B2702p
L
R
(1.46)
(0.99)
(1.03)

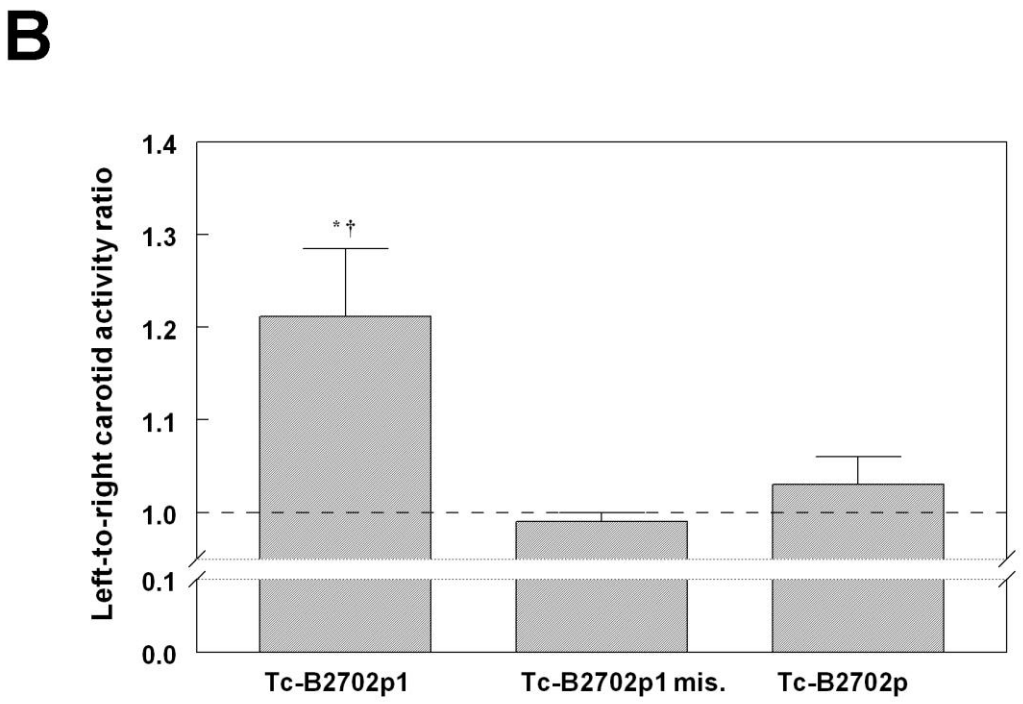
B
Left-to-right carotid activity ratio
1.4
1.3
1.2
1.1
1.0
0.1
0.0
* †
Tc-B2702p1
Tc-B2702p1 mis.
Tc-B2702p

FIGURE 5

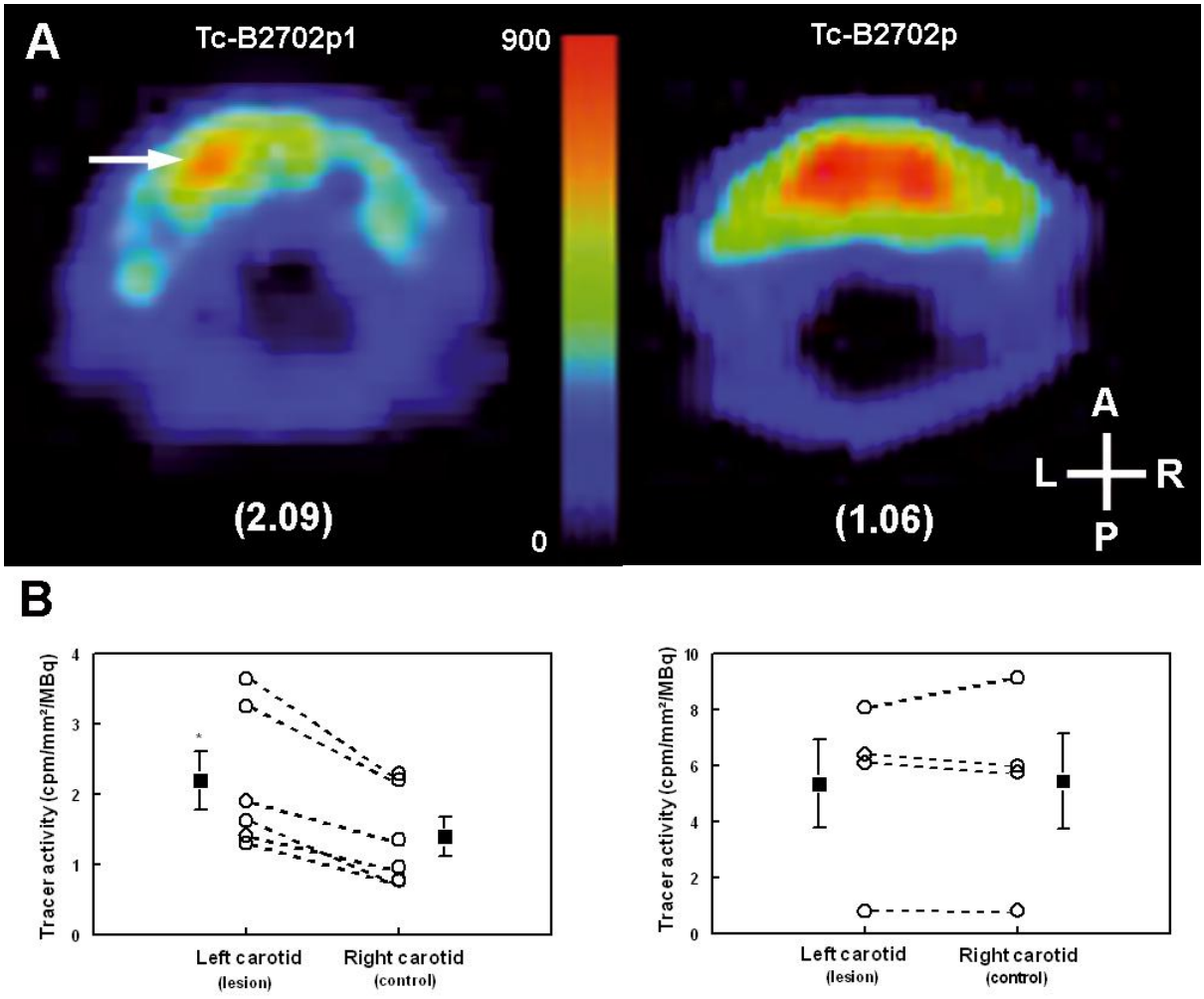
A
Tc-B2702p1
900
0
Tc-B2702p
(2.09)
(1.06)
A
L
R
P
B
Tracer activity (cpm/mm²/MBq)
Left carotid
(lesion)
Right carotid
(control)
Tracer activity (cpm/mm²/MBq)
Left carotid
(lesion)
Right carotid
(control)

FIGURE 6

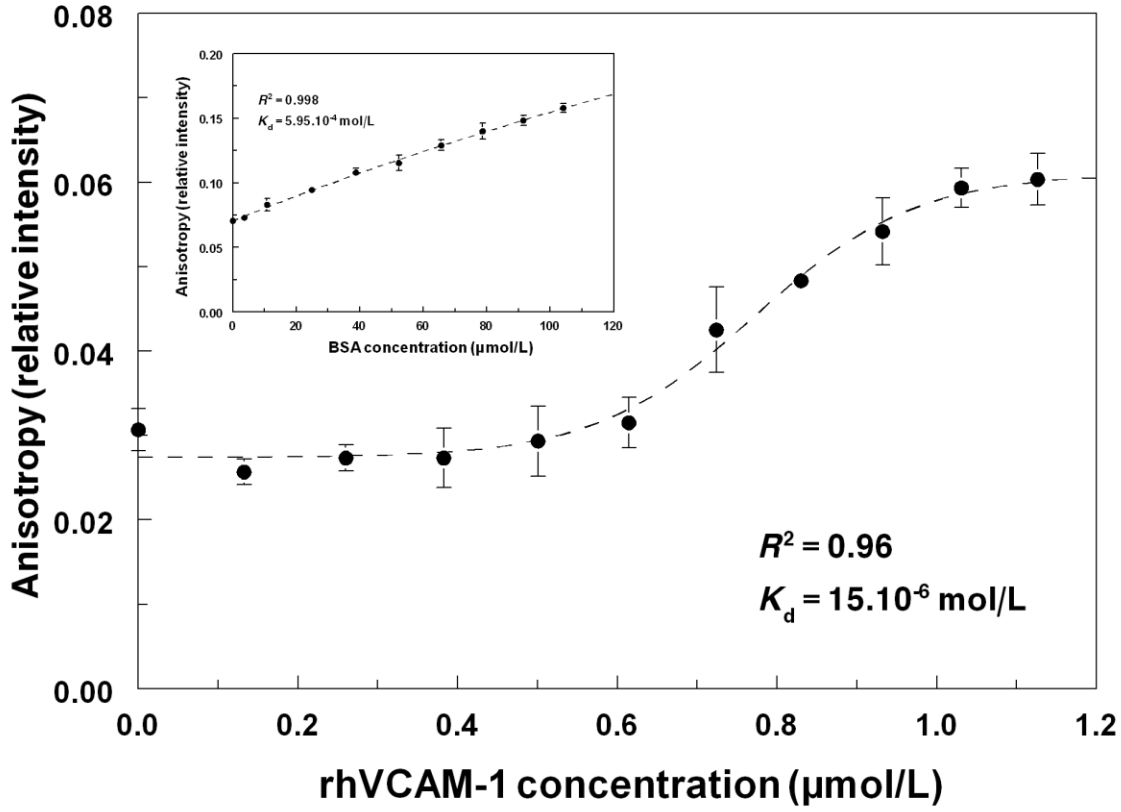
Anisotropy (relative intensity)
rhVCAM-1 concentration (µmol/L)
R^2 = 0.96
K_d = 15.10^{-6} mol/L
Anisotropy (relative intensity)
BSA concentration (µmol/L)
R^2 = 0.998
K_d = 5.95.10^{-4} mol/L